Journal of Nondestructive Evaluation (2020) 39:28
https://doi.org/10.1007/s10921-020-00671-8

Quantitative Evaluation of Deformation Induced Martensite in Austenitic Stainless Steel Using Magnetic NDE Techniques

Esmaeel Ahmadzade-Beiraki[1] · Saeed Kahrobaee[2] · Mehrdad Kashefi[1] · Iman Ahadi Akhlaghi[3] · Mohammad Mazinani[1]

Received: 11 March 2019 / Accepted: 28 February 2020

Abstract
The goal of the present study is to examine the applicability of non-destructive magnetic hysteresis loop technique and Hall effect sensor to characterize the strain induced α′-martensite in an austenitic stainless steel. For this purpose, eight different levels of tensile deformation, from 0.05 to 0.44 true stain values, were applied and corresponding induced martensite fractions were determined, using X-ray diffraction method. Finally, magnetic hysteresis loop and Hall effect methods were applied. Results show that major outputs of hysteresis loop (maximum flux density, retentivity and coercivity) and Hall effect (real part, imaginary part, modulus and phase angle for the 3rd harmonic) are significantly affected by variations in the induced martensite fraction. Besides, a new parameter, amplitude and shape of raw received signal, was used in this study. The established relationships with high correlation coefficients between electromagnetic outputs and martensite fraction indicate the potential of the proposed methods to be used for detecting the microstructural changes in AISI 304 stainless steel subjected to different strains.

Keywords AISI 304 stainless steel · Magnetic hysteresis loop · Hall effect · Harmonic analysis · Strain-induced martensite

1 Introduction

Austenitic stainless steels are utilized in many industrial applications due to their high corrosion resistance and formability. Ductility, strength, resistance to stress corrosion crack and sensitization of the austenitic stainless steels are influenced by deformation induced martensitic transformation in the metastable austenite phase [1–4]. Stability of these steels depends on their chemical composition, temperature, grain size and strain state [4]. Although two potential martensite phases of α′ and ε with BCC and HCP structures respectively can be transformed from austenite, the amount of α′ formation is significantly greater than ε phase [1]. As a result, variations of the steel properties due to the deformation has been mostly attributed to the presence of α′ phase. Although transformation of austenite into α′ results in a great combination of ductility and strength, it inversely degrades the corrosion resistance, in particular, resistance to stress corrosion crack and sensitization [3]. Sensitization of austenitic stainless steels, due to the depletion of alloying elements, results in the formation of martensite along grain boundaries [5] which greatly affect corrosion resistance of the material. Therefore, quantitative evaluation of α′ is of a great importance concerning degradation of austenitic stainless steels.

Conventionally, the amount of α′ is measured, quantitatively, by X-ray diffraction (XRD) method [1, 4, 5], electron backscatter diffraction (EBSD) and optical microscopic observations [6, 7]. The mentioned methods are destructive, expensive and time consuming. Besides, they cannot be employed for 100% inspection process. In contrast, non-destructive techniques are cheaper, faster, and have the ability to be applied in quality control of mass production lines as an efficient tool [8].

Magnetic non-destructive techniques such as hysteresis loop (HL), Barkhausen noise (BN) and eddy current (EC)

✉ Saeed Kahrobaee
Kahrobaee@sadjad.ac.ir

[1] Department of Materials Engineering, Faculty of Engineering, Ferdowsi University of Mashhad, Mashhad, Iran

[2] Department of Mechanical and Materials Engineering, Sadjad University of Technology, Mashhad, Iran

[3] Department of Electrical and Bioelectric Engineering, Sadjad University of Technology, Mashhad, Iran

Published online: 05 March 2020

have been used, particularly, in characterization of various microstructural changes in ferromagnetic steel parts [9–12]. Formation of the ferromagnetic strain-induced martensite phase in paramagnetic austenite matrix enables the magnetic non-destructive evaluation (NDE) methods to be used as the characterization tools in stainless steels. Coercivity as one of the HL outputs has been investigated to detect the martensite phase variations in SS404 austenitic stainless [13] and duplex UNS S32304 [14] steels submitted to cold-working. Application of EC technique for assessment of martensite transformation has been also reported for cold worked AISI 321 stainless steel [15–17]. MBN method has been also introduced to quantitatively measure strain-induced martensite fraction in AISI 304 [17–20] and 301 [21] stainless steels under tensile loads. Variations of electromagnetic properties obtained from HL and EC techniques with respect to the changes in martensite volume fraction have been also investigated in rolled austenitic steels of the 300-series during reverse transformation of martensite to austenite [22–24].

Besides, recent researches show that the various parameters extracted from Fourier transform of input signal of the electromagnetic methods, such as EC, provide important and beneficial information about the magnetic properties, which in turn, could be used to characterize related microstructural features [25–28].

In this paper to characterize the strain induced martensite transformation in austenitic stainless steels, a new magnetic NDE approach has been proposed based on monitoring the magnetic flux leaks from the sample's surface subjected to the an external magnetic field. Whereas, most related studies in this field have been limited to the applications of the MBN, HL and EC methods. The main specifications of the present paper are as follows:

- A new feature of the Hall effect sensor, that indicates the deviation degree of the output signals from the linear state, has been introduced as a useful magnetic parameter in nondestructive characterization of steels. This output parameter represents a significant dependence on amounts of strain-induced α′-martensite created in the austenitic stainless steel.
- The relationships among the characteristics of the Hall effect sensor output and features extracted from hysteresis loop have been evaluated.
- Appling the Fourier transform to the raw signal of Hall effect sensor, important characteristics including real/imaginary parts, relative modulus and phase angle of the first three odd harmonics were determined to be evaluated as a function of martensite fraction changes.

Table 1 Chemical composition of the AISI 304 used in this investigation

Element	C	Cr	Ni	Mn	Cu	Si	P	Fe
Wt%	0.056	16.78	8.719	1.350	0.428	0.598	0.041	Bal.

2 Experimental Procedure

2.1 Sample Preparation and Conventional Characterization Methods

Eight tensile specimens were prepared from 2 mm-thick sheet of AISI 304 austenitic stainless steel, according to the ASTM E8M standard (with 50.0 mm gauge length and 12.50 mm gage width) [29]. The chemical composition of the steel has been presented in Table 1. All the samples were solution treated at 1095 °C for 1 h, and water quenched to room temperature to prevent any carbide precipitation during cooling. To produce different amounts of martensite, the samples were subjected to 0.05, 0.1, 0.15, 0.25, 0.3, 0.35, 0.4, 0.44 true strain values using a Zwick/Z250 tensile testing machine with an average strain rate of 0.002 s^{-1}.

Optical microscopic observations were carried out on the test samples. All samples were electro polished for 40 s at 18 V in an electrolyte bath consisting of 110 ml perchloric acid, 180 ml ethanol and 710 ml methanol. The Beraha's reagent (0.5 g potassium metabisulfite, 20 ml HCl and 100 ml distilled water) was used to reveal martensite phase in the steel microstructures, and the solution of 60% HNO3 in 40% distilled water was employed for etching the grain boundaries. To determine the volume fraction of α′-martensite, XRD quantitative analysis was carried out using Philips X'pert diffractometer with Cu Kα radiation. The quantitative amounts of α′-martensite phases were calculated using Eqs. (1) and (2) presented in the ASTM E975-13 standard [30].

$$V_{\alpha'} = \frac{\left(\frac{1}{n}\right)\sum_{j=1}^{n}\left(\frac{I_{\alpha'}^{j}}{R_{\alpha'}^{j}}\right)}{\left(\frac{1}{n}\right)\sum_{j=1}^{n}\left(\frac{I_{\alpha'}^{j}}{R_{\alpha'}^{j}}\right)+\left(\frac{1}{n}\right)\sum_{j=1}^{n}\left(\frac{I_{\gamma}^{j}}{R_{\gamma}^{j}}\right)}, \tag{1}$$

$$R_{\alpha'/\gamma}^{hkl} = \left(\frac{p\cdot e^{-2M}\cdot F^{2}}{v^{2}}\right)\left(\frac{1+\cos^{2}2\theta}{\sin^{2}\theta\cdot\cos\theta}\right), \tag{2}$$

where n, I and R_i are the number of peaks for each phase, the integrated intensity of the reflecting plane and the material scattering factor (R_i), respectively. Values of R_i were calculated from Eq. (2), where V is the volume of unit cell, F is the structure factor, p is the multiplicity factor and e^{-2M} is the temperature factor.

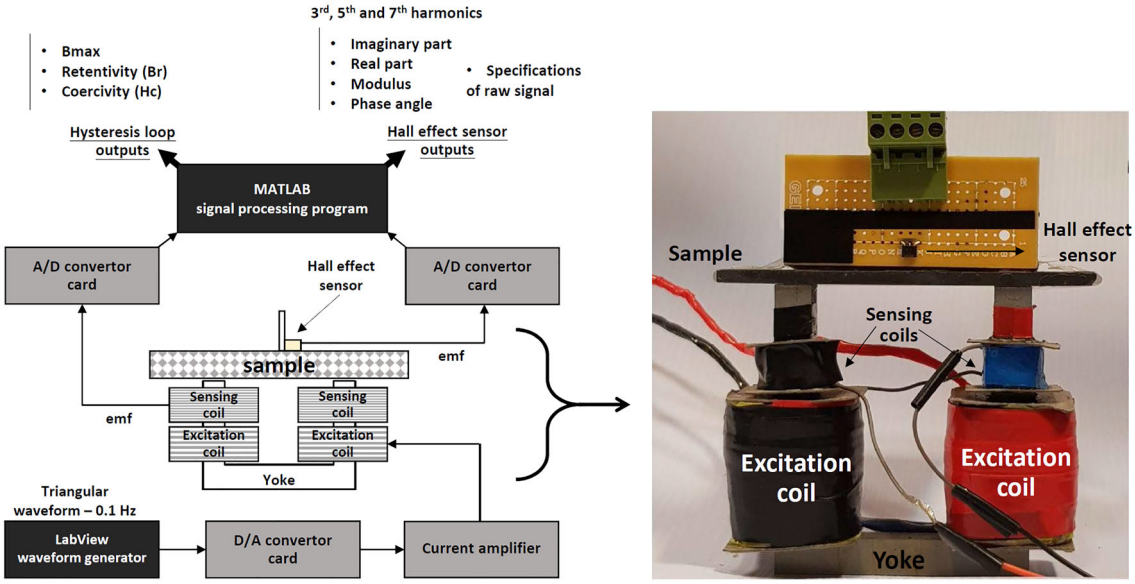

Fig. 1 Schematic block diagram and U-shaped magnetic sensor/Hall effect sensor of the NDE system proposed for characterizing the martensite fraction

2.2 Nondestructive Characterization Methods

Magnetic hysteresis loop (HL) and Hall effect (HE) techniques, were used to determine the electromagnetic responses to the formation of strain-induced martensite under the external magnetic field. The schematic block diagram of the whole system is depicted in Fig. 1. For both the HE and HL measuring systems, the same two concatenated exciting coils with 1500 turns of fine copper wire were used to magnetize the samples. Each of these coils was wound on an arm of a U-shape yoke and a triangular waveform was used to drive them. The amplitude and frequency of the waveform (0.1 Hz) could be adjusted in a LabVIEW program. A two-stage bi-polar amplifier, which is originally designed and utilized for this project, was used to amplify the current of the waveform received from the Advantech PCI-1720U-AE D/A conversion card analog port. The amplifier can provide 1 A current, which guaranties the samples would be magnetically saturated.

In the HL system, two in-series sensing coils with 1000 turns of finer copper wire wound on the aforementioned yoke, were used to measure the induced magnetic field. In order to measure the surface field in the HE method, a Hall sensor (HW-108C) was located 1 mm above the sample. The outputs of the sensing coils and Hall sensor were fed to the Advantech PCI-1714UL-BE A/D conversion card and sampled with the depth of 12 bits and the sampling rate of 500 Hz. In order to obtain the B-field, the induced voltage (emf) is time-integrated and scaled using a MATLAB program. The H-field is determined by scaling the driving current amplitude, taken from the LabVIEW program. H and B-fields are then used to depict the hysteresis loop.

Besides, the raw HE signals are processed using a MATLAB signal processing program. Peak-to-peak amplitude values (Vp-p) and the slopes of the raw HE signals at zero-crossing points were used to classify the samples. Finally, Fourier transform of the input signal was used to determine the real/imaginary parts, relative modulus and phase angle of the first three odd harmonics (3rd, 5th and 7th). These parameters are defined in Eqs. (3)–(6) [31].

$$X_i^j = \text{real}\left\{ \text{FFT}\left[x_{HE}^j(t)\right]\Big|_{f=f_i} \right\}, \tag{3}$$

$$Y_i^j = \text{imaginary}\left\{ \text{FFT}\left[x_{HE}^j(t)\right]\Big|_{f=f_i} \right\}, \tag{4}$$

$$\Delta m_i^j = \text{abs}\left\{ \text{FFT}\left[x_{HE}^j(t)\right]\Big|_{f=f_i} \right\} - \text{abs}\left\{ \text{FFT}\left[x_{HE}^0(t)\right]\Big|_{f=f_i} \right\} \tag{5}$$

$$\Delta m_i^j = \angle\left\{ \text{FFT}\left[x_{HE}^j(t)\right]\Big|_{f=f_i} \right\} - \angle\left\{ \text{FFT}\left[x_{HE}^0(t)\right]\Big|_{f=f_i} \right\} \tag{6}$$

where $x_{HE}^j(t)$ is the hall sensor signal for the jth sample, FFT [.] is a function that computes the Fast Fourier Transform (FFT) of its input signal and f_i is the frequency of the ith harmonic.

3 Results and Discussion

3.1 Microstructural Characterization

Figure 2 shows optical microscopic images from the samples subjected to different amounts of strains. As shown in Fig. 2a, a few dark areas representing α′-martensite (strain-induced martensite) phase in light austenitic matrix are observed even

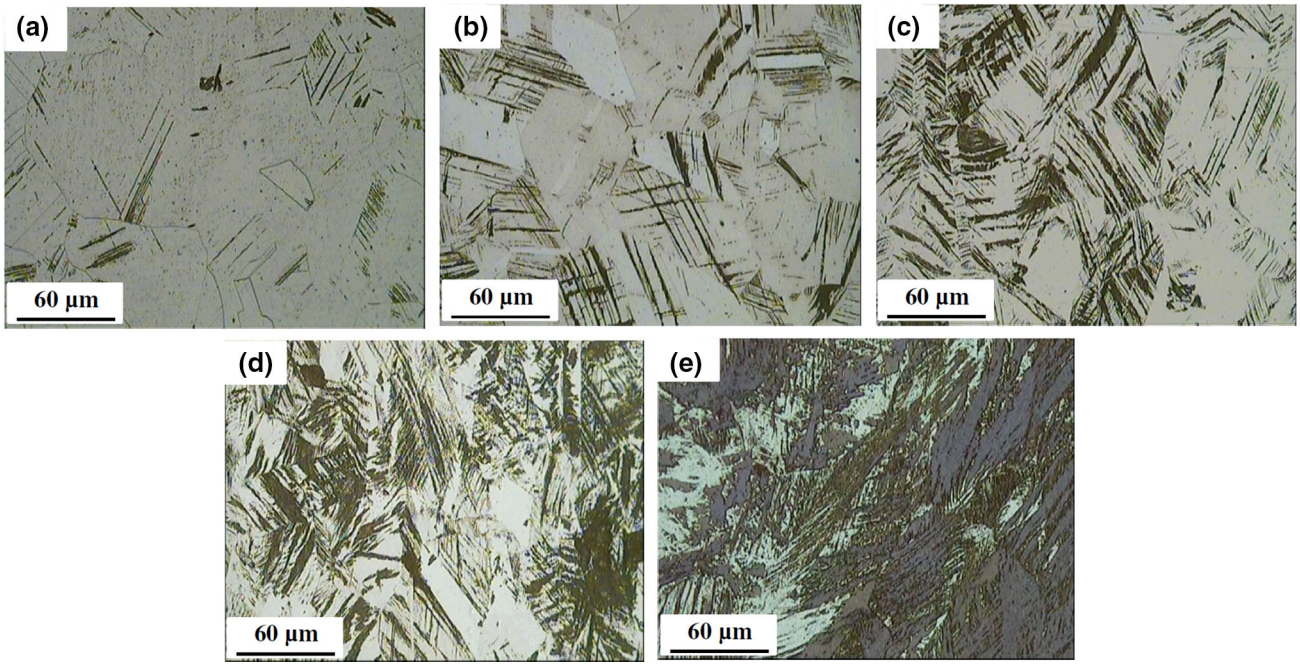

Fig. 2 Optical micrographs showing α′-martensite phase formed in the samples under true strain values of **a** 0.05, **b** 0.15, **c** 0.25, **d** 0.35, and **e** 0.44

after 0.05 true strain. Comparing the Fig. 2a–d indicates that as the deformation proceeds thin martensite laths are randomly formed within the austenitic grains and finally, for the sample with 0.44 strain (Fig. 2e), extensive transformation is observed.

XRD spectra of the samples submitted to various strains have been presented in Fig. 3. As it can be seen, by applying the first step of plastic deformation (true strain of 0.05), in addition to the four characteristic austenite peaks corresponding to 2θ angles of 43.47°, 50.67°, 74.67°, and 90.67°, another peak is also created at 44.67°. This is related to (110) plane of α′ martensite. Applying 0.1 true strain, two other peaks corresponding to (200) and (211) planes of α′ martensite phase have been respectively created at 2θ angles of 65.02° and 82.33°. Figure 3 clearly shows that as the strain increases, the intensity of the peaks associated with the martensite phase increases, while the peaks of the austenite phase are reduced. The quantitative values of martensite fraction calculated using Eqs. (1) and (2) (defined in 2.1 section) have been demonstrated in Fig. 4. As it can be seen, increasing the strain from 0.05 to 0.44, results in an increase of the volume percentage of induced martensite fraction from 8.8% to 80%. Figure 4 also indicates an increase in hardness as a function of true strain due to the enhancement of martensite volume fraction. Martensite is a harder phase than austenite, and as a result, the hardness of sample increases with plastic deformation. The hardness of samples increases from 173 ($\alpha' = 9\%$) to 389 Vickers ($\alpha' = 80\%$). Similar results have been reported by Mészáros and Prohászka [32].

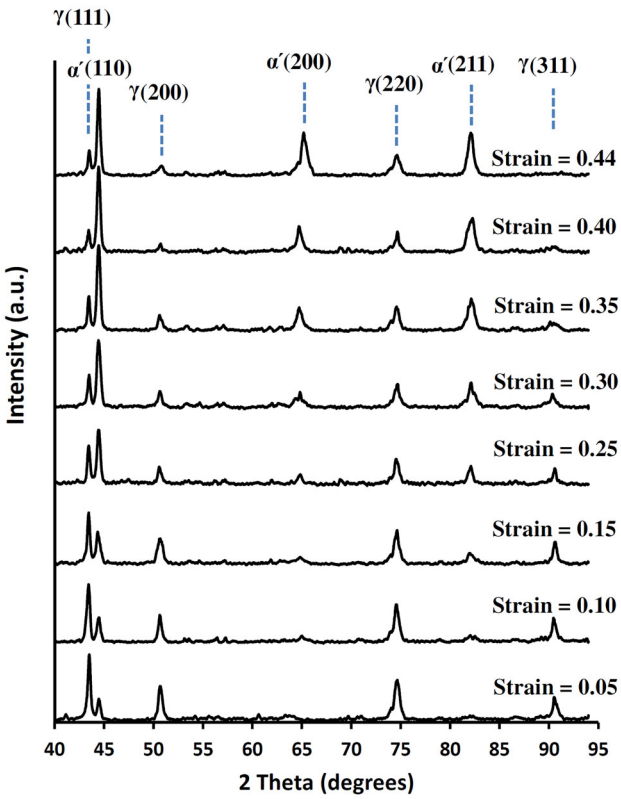

Fig. 3 XRD patterns for the samples under various true strains

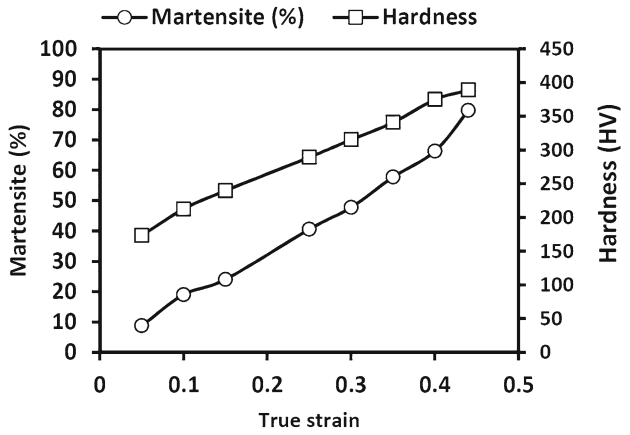

Fig. 4 Variations of martensite percentage estimated from XRD patterns and hardness with true strain

3.2 Non-destructive Evaluations

Figure 5 demonstrates the variations of HL outputs as a function of martensite fraction induced in austenitic matrix of the test samples. As it can be seen, the same increasing trend has been obtained for all the HL outputs. This is attributed to the more favourable response of ferromagnetic martensite phase to the applied magnetic field compared to the paramagnetic austenite one. Therefore, a stronger magnetic behaviour is expected in magnetization curve of the samples containing higher volume percentages of the martensite phase. This changes in magnetic response increases the max. flux density (Bmax) as well as retentivity (Br) and coercivity (Hc) of the samples. In cold worked austenitic stainless steels, three phases, with different magnetic properties, are presented. These phases include austenitic matrix, ε-martensite which forms on close-packed (111) planes in the austenite with HCP crystal structure and the BCT α′-martensite which forms as plates with (225) habit planes in groups bound by faulted sheets of austenite on (111) planes [33, 34]. Fourlaris and Gladman [35] by characterizing microstructure of a 302 type metastable austenitic stainless steel subjected to 18% cold deformation, indicated that magnetic domain boundaries are only present within the lath region of an α′-martensite packet area, whereas paramagnetic austenite and ε-martensite regions are free of domain boundaries. Obviously, increasing the size and amount of martensitic clusters at larger strains, higher volume of the material is subjected to domain wall movement.

The raw outputs of the Hall sensor versus time have been shown in Fig. 6a, for eight samples with different martensite volume fraction. As the figure shows, these signals have different amplitudes and hence, the peak-to-peak amplitude values (Vp-p) could be used to distinguish the samples. Moreover, for different samples, the slopes of the curves at zero-crossing points are not the same. Therefore, it is also possible to utilize these values to discern samples with different martensite volume fractions. To do so, time derivative of the Hall sensor signal would be used. Figure 6b shows that the depth of the valleys corresponding to the zero crossing points (β), clearly depends on the martensite fraction of the samples.

The variations of Vp-p and β with respect to the martensite fraction have been presented in Fig. 7. The increasing trend of Vp-p and β obtained from the raw triangular signals is, respectively, due to the higher amount of magnetic flux sensed by the HE sensor and higher amounts of Br and Hc for samples with higher volume fraction of martensite. For both Vp-p and β, high correlation coefficients ($R^2 = 0.93$ and

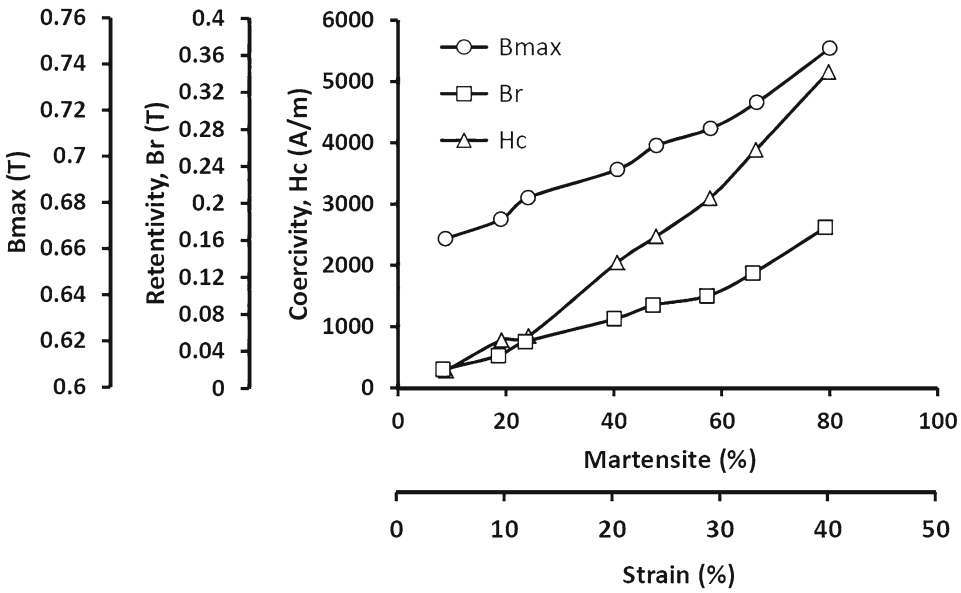

Fig. 5 Variations of HL outputs including Bmax, Br, and Hc, as a function of martensite fraction

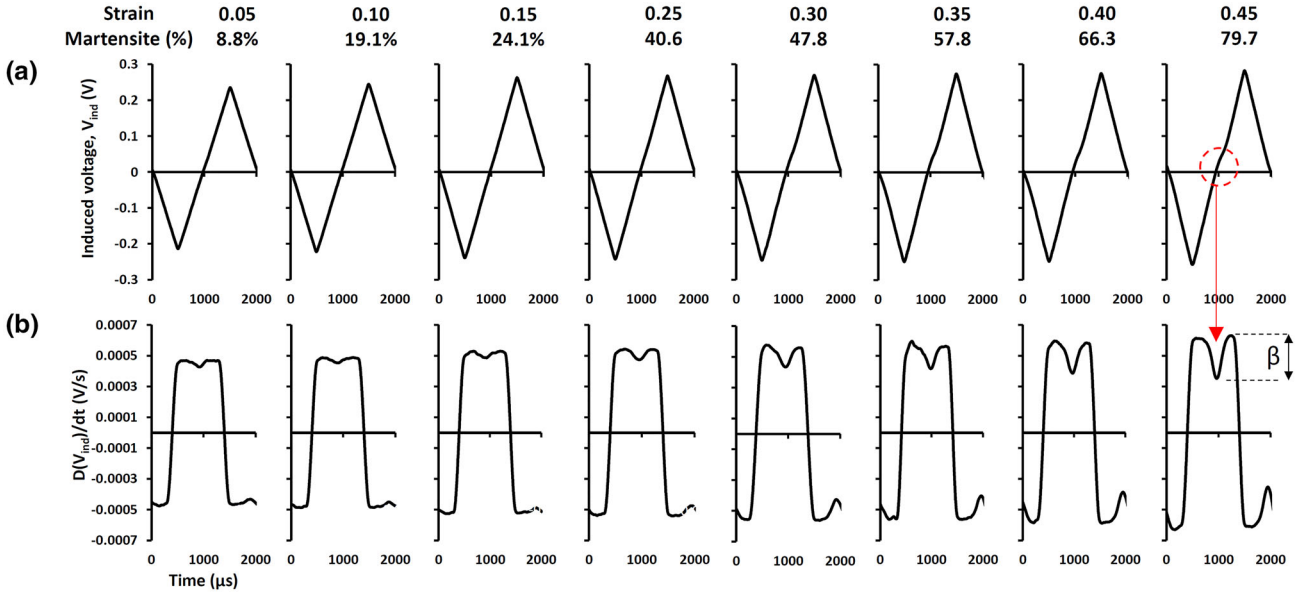

Fig. 6 **a** Induced voltage (V_{ind}) and **b** its time derivative (dV_{ind}/dt) as a function of time, for samples subjected to the various stains (with different amounts of martensite fraction)

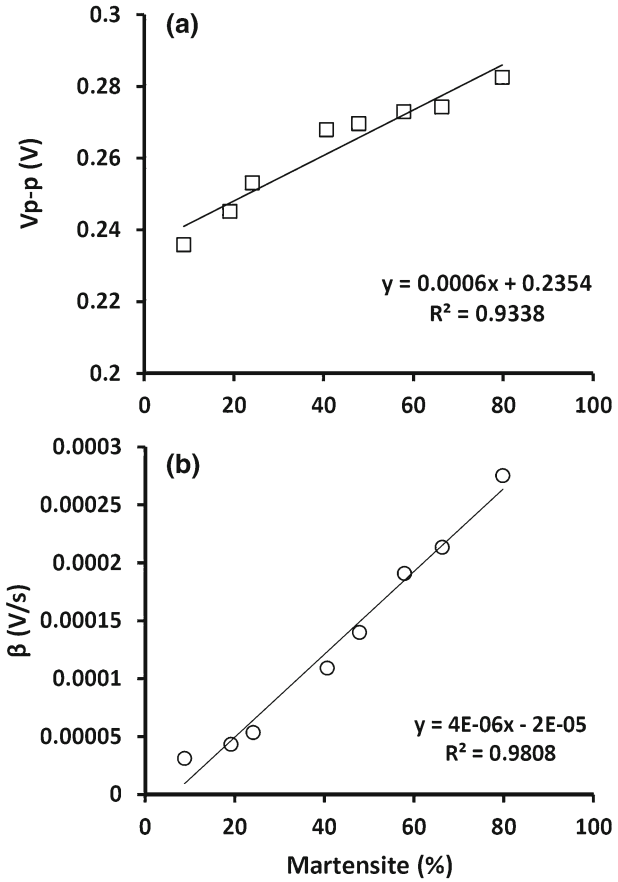

Fig. 7 Variations of **a** Vp-p and **b** β, as a function of martensite percentage

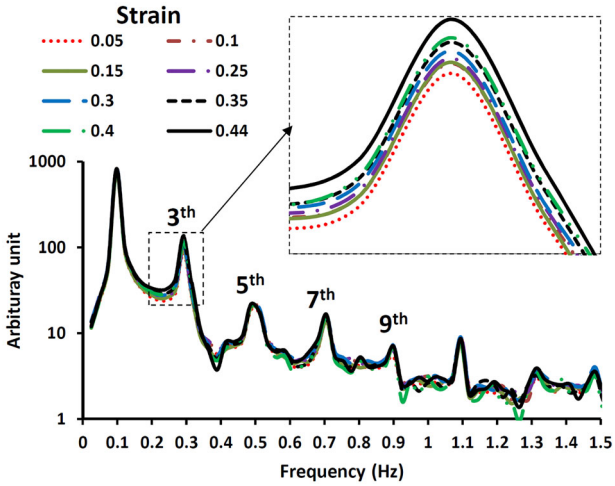

Fig. 8 Fourier transform amplitude of the Hall sensor signal for 3rd, 5th and 7th harmonics for five samples with different martensite fraction

$R^2 = 0.98$, respectively) have been obtained from the linear regression.

Amplitude of the Fourier transform of the Hall sensor signal for odd harmonics as a function of frequency is also presented in Fig. 8. The first harmonic relates to the main applying frequency, and other odd harmonics may be formed due to the presence of a ferromagnetic material in the vicinity of the applied magnetic field. In fact, the presence of odd harmonics is influenced by the degree of nonlinearity of hysteresis loop and the magnitude of applied magnetic field [21]. Therefore, it can be concluded that the HE outputs are affected by the magnetic hysteresis behavior of the samples.

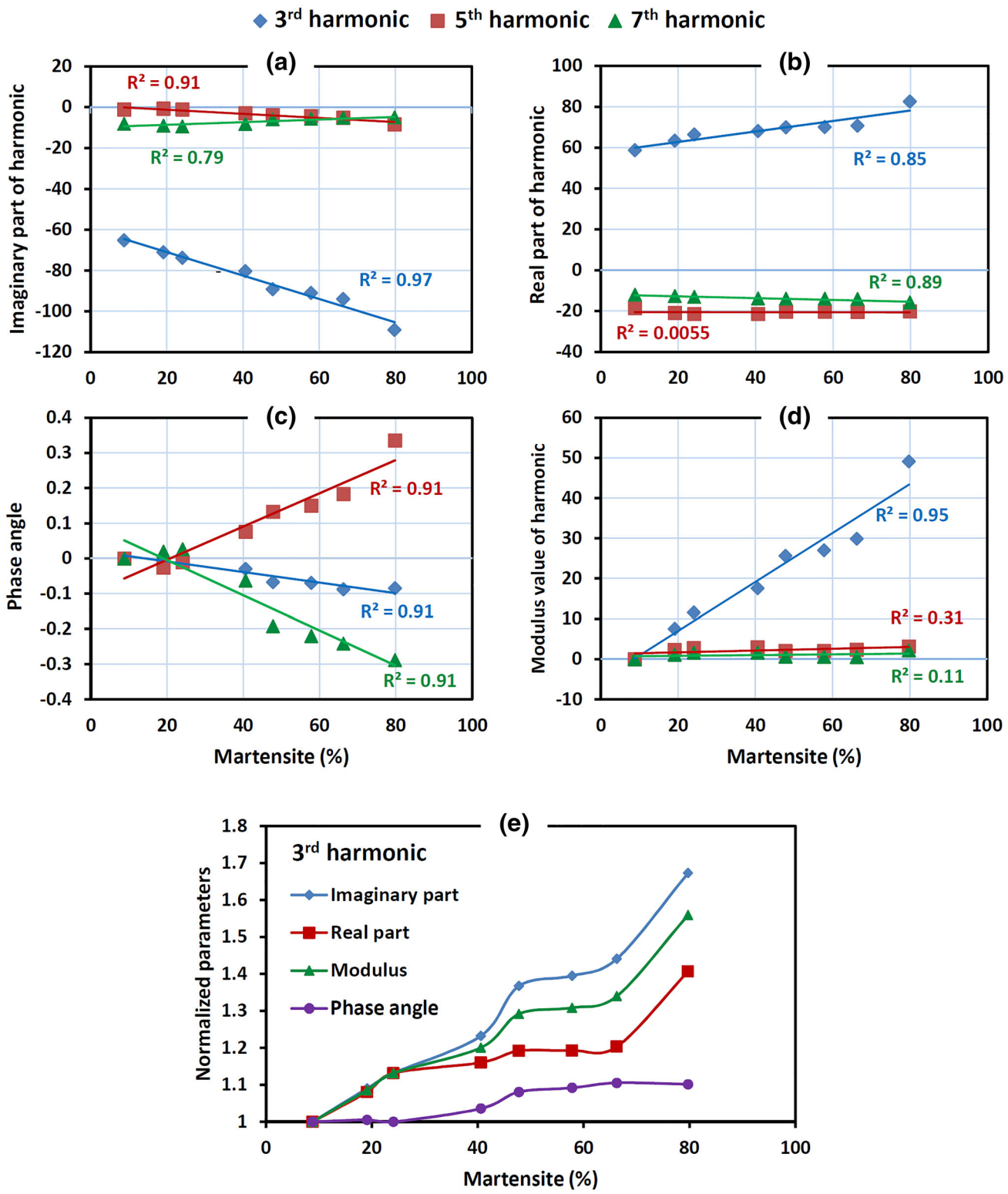

Fig. 9 Variations of **a** imaginary part, **b** real part, **c** relative phase angle, and **d** relative modulus value for the 3rd, 5th and 7th harmonics and **e** normalized values of the parameters for the 3rd harmonic, as a function of martensite volume fraction

The relationships between values of the real and imaginary parts as well as relative modulus and phase angle of 3rd, 5th and 7th harmonics and martensite percentage have been depicted in Fig. 9. The figure indicates that apart from the phase angle (Fig. 9c), for the other parameters, the values obtained from harmonic 3 could be used to successfully dis-

tinguish samples. For phase angle variations, the values for all the harmonics have been varied significantly, as a result of increasing in martensite fraction. Besides, the high correlation obtained from linear relationships for the real part ($R^2 = 0.97$), imaginary part ($R^2 = 0.85$), phase angle ($R^2 = 0.91$) and modulus value ($R^2 = 0.95$) of harmonic 3 show the capability of the harmonic analysis to determine the martensite volume fraction.

In order to have a better understanding on the effect of martensite volume fraction on the values of the real and imaginary parts as well as modulus and phase angle of 3rd harmonic, their normalized values were evaluated by dividing the values of each parameter to the one for the sample with minimum martensite percentage (8.8%). Figure 9e shows the increasing trends for all the normalized parameters with martensite fraction. Considering Eqs. 7 and [8], it can be concluded that increasing in magnetic permeability (μ) results in increasing of induction resistance (X) which is equal to the value of imaginary part. Besides, formation of martensite phase in austenitic matrix causes an increase in the resistance [36]. Therefore, higher values of X and R (which is equal to the real part amplitude) could be achieved for the samples containing higher martensite phase.

$$X = 2\pi f\left(\mu N^2 A/l\right) \tag{7}$$

where f is the frequency, μ is the magnetic permeability, N is the number of turns around the coil, A is the cross-section area and l is the coil length. Considering Eqs. (8) and (9) and $Z = R + jX_L$ ([28], the increasing trend of modulus and phase angle with martensite fraction is justified. The ascending trend with low slope for phase angle is due to the dominant effect of the imaginary part.

$$\text{modulus}\,(Z) = \text{abs}\,(Z) = \sqrt{[\text{real}\,(Z)]^2 + \left[\text{imaginary}\,(Z)\right]^2} \tag{8}$$

$$\text{phase angle}\,(Z) = \measuredangle(Z) = \tan^{-1}\left[\frac{\text{imaginary}\,(Z)}{\text{real}\,(Z)}\right] \tag{9}$$

From practical point of view, it should be noted that the excitation and sensing coils and Hall effect sensor could be banded together in a single probe to simultaneously measure all required electromagnetic parameters. Besides, in the data analysis phase, in addition to the separate correlation among each parameter and martensite fraction, fusion of all parameters could also provide higher prediction accuracy. As a limitation of the proposed method, one can notice that it could be used only for the austenitic stainless steel samples with a constant thickness and chemical composition. However, since in the mass production of industrial products, thickness and chemical composition of the parts are constant, this is not an important limitation. Moreover, if any change in thickness and chemical composition is occurred, only a simple new calibration needs to be performed to accommodate the new conditions.

4 Conclusion

The aim of the present investigation is to evaluate the relationships between the microstructural changes induced in AISI 304 stainless steel submitted to the various amounts of tensile loads and their corresponding magnetic properties. The most important results are as follow.

1. Applying strain from 0.05 to 0.44 by tensile testing creates strain-induced martensite from 8.8% to 80%.
2. Increase in amount of ferromagnetic martensite phase in paramagnetic austenite matrix increases all the outputs extracted from magnetic hysteresis loop (maximum flux density, retentivity and coercivity).
3. The amplitude and shape of the received raw signal from Hall effect sensor are affected by increase in induced martensite volume fraction. Besides, the depth of valleys in the time derivative of Hall sensor signal (at HE signal zero crossing points) is found as the optimum NDE parameter, which is suggested to be used for monitoring the martensite fraction.
4. High correlation coefficients are also found between the real part, imaginary part, relative modulus and relative phase angle for the 3rd harmonic and martensite fraction.

References

1. Lebedev, A., Kosarchuk, V.: Influence of phase transformations on the mechanical properties of austenitic stainless steels. Int. J. Plast. **16**(7–8), 749–767 (2000)
2. Spencer, K., Embury, J., Conlon, K., Veron, M., Bréchet, Y.: Strengthening via the formation of strain-induced martensite in stainless steels. Mater. Sci. Eng., A **387**, 873–881 (2004)
3. Briant, C., Ritter, A.: The effects of deformation induced martensite on the sensitization of austenitic stainless steels. Metall. Trans. A **11**(12), 2009–2017 (1980)
4. Talonen, J.: Effect of strain-induced α′-martensite transformation on mechanical properties of metastable austenitic stainless steels. Doctoral Dissertation, Helsinki University of Technology, Espoo, Finland (2007)
5. Kamada, Y., Mikami, T., Takahashi, S., Kikuchi, H., Kobayashi, S., Ara, K.: Compositional dependence of magnetic properties on thermally sensitized austenitic stainless steels. J. Magn. Magn. Mater. **310**(2), 2856–2858 (2007)
6. Haušild, P., Davydov, V., Drahokoupil, J., Landa, M., Pilvin, P.: Characterization of strain-induced martensitic transformation in a metastable austenitic stainless steel. Mater. Des. **31**(4), 1821–1827 (2010)
7. Beese, A.M., Mohr, D.: Experimental quantification of phase transformation in austenitic stainless steel. In: Proceedings of the SEM 2009 Annual Conference & Exposition on Experimental & Applied Mechanics, 2009

8. Shull, P.J.: Nondestructive Evaluation: Theory, Techniques, and Applications. CRC Press, Boca Raton (2002)
9. Kahrobaee, S., Haghighi, M.S., Akhlaghi, I.A.: Improving nondestructive characterization of dual phase steels using data fusion. J. Magn. Magn. Mater. **458**, 317–326 (2018)
10. Nezhad, K.K., Kahrobaee, S., Akhlaghi, I.A.: Application of magnetic hysteresis loop method to determine prior austenite grain size in plain carbon steels. J. Magn. Magn. Mater. **324**(23), 4090–4093 (2019)
11. Kahrobaee, S., Norouzi Sahraei, H., Ahadi Akhlaghi, I.: Nondestructive characterization of microstructure and mechanical properties of heat treated H13 tool steel using magnetic hysteresis loop methodology. Res. Nondestruct. Eval. **30**(1), 1–13 (2019)
12. Altpeter, I., Tschuncky, R., Szielasko, K.: Electromagnetic techniques for materials characterization. In: Huebschen, G., Altpeter, I., Tschuncky, R., Herrmann, H.-G. (eds.) Materials Characterization Using Nondestructive Evaluation (NDE) Methods, pp. 225–262. Elsevier, New York (2016)
13. O'sullivan, D., Cotterell, M., Meszaros, I.: The characterisation of work-hardened austenitic stainless steel by NDT micro-magnetic techniques. NDT and E Int. **37**(4), 265–269 (2004)
14. Mendonça, C., Matos, R., Mendes, J., Melo, M., Rodrigues, G., da Silva, M., Silva, G.: Study of formation and reversion of the martensitic phase induced by deformation of lean duplex stainless steel. J. Nondestruct. Eval. **37**(3), 64 (2018)
15. Liu, K., Zhao, Z., Zhang, Z.: Eddy current assessment of the cold rolled deformation behavior of AISI 321 stainless steel. J. Mater. Eng. Perform. **21**(8), 1772–1776 (2012)
16. Khan, S., Ali, F., Khan, A.N., Iqbal, M.: Eddy current detection of changes in stainless steel after cold reduction. Comput. Mater. Sci. **43**(4), 623–628 (2008)
17. Shaira, M., Guy, P., Courbon, J., Godin, N.: Monitoring of martensitic transformation in austenitic stainless steel 304 L by eddy currents. Res. Nondestruct. Eval. **21**(2), 112–126 (2010)
18. Astudillo, M.R.N., Nicolás, M.N., Ruzzante, J., Gómez, M.P., Ferrari, G.C., Padovese, L.R., Pumarega, M.I.L.: Correlation between martensitic phase transformation and magnetic Barkhausen noise of AISI 304 steel. Procedia Mater. Sci. **9**, 435–443 (2015)
19. Vincent, A., Pasco, L., Morin, M., Kleber, X., Delnondedieu, M.: Magnetic Barkhausen noise from strain-induced martensite during low cycle fatigue of 304L austenitic stainless steel. Acta Mater. **53**(17), 4579–4591 (2005)
20. Ahmadzade-Beiraki, E., Mazinani, M., Kashefi, M.: Examination of Barkhausen noise parameters for characterisation of strain-induced martensitic transformation in AISI 304 stainless steel. Insight-Non-Destruct. Test. Cond. Monit. **58**(6), 297–301 (2016)
21. Haušild, P., Kolařík, K., Karlík, M.: Characterization of strain-induced martensitic transformation in A301 stainless steel by Barkhausen noise measurement. Mater. Des. **44**, 548–554 (2013)
22. Savin, A., Fava, J., Spinosa, C., Ruch, M., Landau, M., Carabedo, F., Cosarinsky, G., Steigmann, R., Craus, M.: Study of the reverse martensitic transformation using non-destructive electromagnetic and materials characterization techniques. Electromagn. Nondestruct. Eval. **42**, 67 (2017)
23. Fava, J., Spinosa, C., Ruch, M., Carabedo, F., Landau, M., Cosarinsky, G., Savin, A., Steigmann, R., Craus, M.L.: Characterization of reverse martensitic transformation in cold-rolled austenitic 316 stainless steel. Matéria (Rio de Janeiro) (2018). https://doi.org/10.1590/s1517-707620180002.04
24. Ruch M, Fava J, Spinosa C, Landau M, Cosarinsky G, Savin A, Novy F, Turchenko V, Craus M Characterization of cold rolling-induced martensite in austenitic stainless steels. In: Proceedings of the 19th World Conference on Non-Destructive Testing 2016, 2016, pp 13–17
25. Ghanei, S., Kashefi, M., Mazinani, M.: Eddy current nondestructive evaluation of dual phase steel. Mater. Des. **50**, 491–496 (2013)
26. Klümper-Westkamp, H., Zoch, H.-W., Reimche, W., Bach, F.: High temperature resistant eddy current sensor for "in situ" monitoring the material microstructure development of steel alloys during heat treatment–bainite sensor. Procedia Eng. **25**, 1605–1608 (2011)
27. Kwun, H., Burkhardt, G.L.: Nondestructive measurement of stress in ferromagnetic steels using harmonic analysis of induced voltage. NDT Int. **20**(3), 167–171 (1987)
28. Mercier, D., Lesage, J., Decoopman, X., Chicot, D.: Eddy currents and hardness testing for evaluation of steel decarburizing. NDT E Int. **39**(8), 652–660 (2006)
29. Standard A E8/E8M: Standard test methods for tension testing of metallic materials **3**, 66 (2011)
30. E975-13 A: Standard practice for X-ray determination of retained austenite in steel with near random crystallographic orientation. In: Proceedings of the ASTM West Conshohocken, PA, 2013
31. Oppenheim, A.V., Willsky, A.S., Young, I.T.: Signals and Systems. Prentice-Hall, Englewood Cliffs (1983)
32. Mészáros, I., Prohászka, J.: Magnetic investigation of the effect of α′-martensite on the properties of austenitic stainless steel. J. Mater. Process. Technol. **161**(1–2), 162–168 (2005)
33. Mataya, M., Carr, M., Krauss, G.: The Bauschinger effect in a nitrogen-strengthened austenitic stainless steel. Mater. Sci. Eng. **57**(2), 205–222 (1983)
34. Vértesy, G., Tomáš, I., Mészáros, I.: Non-destructive indication of plastic deformation of cold-rolled stainless steel by magnetic adaptive testing. J. Magn. Magn. Mater. **310**(1), 76–82 (2007)
35. Fourlaris, G., Gladman, T.: Microscopical characterisation of martensite formation in a metastable austenitic stainless steel. J. Phys. IV Colloq. **7**(C5), C5-423–C5-428 (1997)
36. Kahrobaee, S., Kashefi, M.: Microstructural characterization of quenched AISI D2 tool steel using magnetic/electromagnetic nondestructive techniques. IEEE Trans. Magn. **51**(9), 1–7 (2015)